

大厚度 TC21 钛合金电子束焊接试验

张秉刚¹, 王 廷¹, 陈国庆¹, 刘成来², 刘玉龙¹

(1. 哈尔滨工业大学 现代焊接生产技术国家重点实验室, 哈尔滨 150001;

2. 沈阳黎明航空发动机(集团)有限责任公司, 沈阳 110000)

摘 要: 对 56 mm 厚 TC21 钛合金进行了电子束对接试验, 对接头显微组织和力学性能进行了研究. 结果表明, 接头焊缝区组织形态以柱状 β 晶粒为基体, 针状的马氏体弥散其中; 热影响区从焊缝到母材分为三个区域, 依次为等轴再结晶 β 晶粒区、片状和针状 α 相形成的魏氏组织区以及片状 α 相聚集长大的区域; 熔合区内柱状晶与等轴晶共生. 接头强度达到母材水平, 断裂发生在母材内, 接头厚度方向性能一致. 接头塑性损失较大, 只达到母材的 50% 左右. 接头焊缝区硬度最高, 其次是热影响区的等轴晶区和魏氏组织区, 而热影响区内片状 α 相聚集长大的区域硬度值最低.

关键词: TC21 钛合金; 电子束焊接; 显微组织; 力学性能

中图分类号: TG456.3 **文献标识码:** A **文章编号:** 0253-360X(2009)11-0005-04



张秉刚

0 序 言

钛合金作为一种优良的结构材料具有高的比强度、比刚度、极强的抗腐蚀性, 广泛应用于工业生产的各个领域^[1]. 随着现代工业及国防装备的日趋大型化, 超厚板焊接金属结构的应用愈来愈广泛, 因此大厚度钛合金焊接技术的研究对于现代工业以及国防技术的发展具有重要推动作用.

电子束焊接(electron beam welding, EBW)具有焊接效率高、穿透能力强、焊接变形小以及焊缝保护好等优点, 已经成功地进行了多种钛合金的电子束焊接^[2-6]. 但目前对于大厚度(厚度大于 40 mm)钛合金板材电子束焊接的研究还相对较少.

文中对 56 mm 厚 TC21 钛合金板的电子束焊接进行了研究, 分析了接头的显微组织和力学性能, 为大厚度 TC21 钛合金电子束焊接在工业中的应用提供了试验基础.

1 试验方法

试验所用材料为国产新型 TC21 钛合金, 厚度为 56 mm. 其化学成分和力学性能见表 1. 焊前对试板对接面进行清理. 焊接工艺参数为加速电压 55 kV, 聚焦电流 2 060 mA, 电子束束流 425 mA, 焊接速度

500 mm/min, 电子束扫描幅值 4.0 mm, 扫描频率 300 Hz, 电子束焦点位于表面以下 1/3 处.

表 1 TC21 钛合金化学成分和力学性能

Table 1 Chemical composition and mechanical properties of TC21 titanium alloy

化学成分(质量分数, %)										力学性能	
Al	Sn	Zr	Mo	Cr	Nb	Fe	Si	Ti	余量	抗拉强度 R_m / MPa	断后伸长率 A (%)
6.2	2.1	1.7	3.0	1.7	1.9	0.1	0.1	余量		1 090	49

焊后沿垂直焊接方向在接头不同厚度位置截取金相试样, 采用 PMG3 OLYMPOS 光学显微镜分析了显微组织形貌, 在 INSTRON MODEL1186 电子万能试验机上进行拉伸试验, 拉伸试样分别从接头的不同厚度位置截取(图 1), 以研究大厚度钛合金电子束

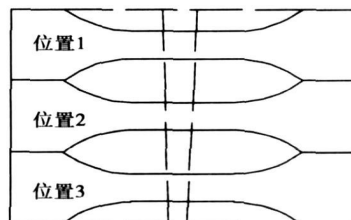


图 1 拉伸试样取样位置

Fig 1 Sampling locations of tensile samples

焊接时厚度方向上的力学性能差异. 采用 HV-100 型显微硬度计对接头横截面水平方向和垂直方向的显微硬度分布进行了测量.

2 试验结果及分析

2.1 接头宏观形貌

图2为接头的宏观形貌. 从图2中可以看出焊缝未出现缺陷, 接头整体成形良好. 从图2中还可以看到焊缝宽度在竖直方向上有明显的变化, 呈现出上宽下窄的特征. 在上表面处, 焊缝宽度约为7 mm, 而在下表面处, 焊缝宽度减小为约4 mm, 焊缝这种宽度差异很可能导致性能上的差异. 焊缝深宽比约为10:1. 接头热影响区较窄, 约2 mm. 与传统电弧焊类似, TC21 电子束焊接接头也明显的分为焊缝区、熔合区、热影响区以及未受影响的母材.

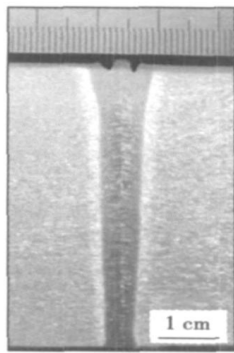


图2 接头横截面宏观形貌

Fig. 2 Macrostructure in cross-section of joint

2.2 接头各区域显微组织形貌

2.2.1 母材

图3为TC21的显微组织形貌. 从图3中可见, TC21显微组织为双相钛合金常用的网篮组织, 原始的 β 相界在热加工中破碎, 有少量的晶界 α 相

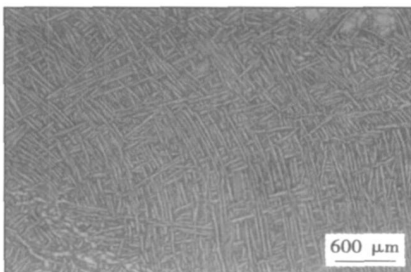


图3 TC21 显微组织形貌

Fig. 3 Microstructure of TC21

存在, 大部分 α 相为短小的片状, 分布在 β 相基体内.

2.2.2 焊缝区

图4为接头焊缝区的显微组织形貌. 从图4中可以看出, 焊缝为凝固形成的粗大 β 柱状晶, 由焊缝两侧向焊缝中心生长, 并在焊缝中心破碎, 成为新的形核质点, 长大成为细小的 β 等轴晶. 图5为 β 晶内的显微组织形貌. 从图5中可以看出, β 晶粒内部为快冷形成的 α' 马氏体针. 这是由于电子束焊接过程中冷却速度很大, β 相来不及通过原子扩散转变成平衡态的 α 相, 只能发生切变相变, 生成针状含过饱和 α 相稳定元素的马氏体 α' . 但是由于金属中的合金元素含量很高, β 相在冷却过程中并不能完全转变为马氏体 α' , 大部分以亚稳 β -Ti的形式存在, 因此焊缝最终的组织形态为以亚稳 β 相为基体, 针状的马氏体 α' 相弥散在其中.

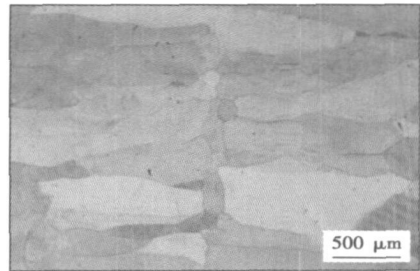


图4 焊缝区显微组织形貌

Fig. 4 Microstructure of weld zone

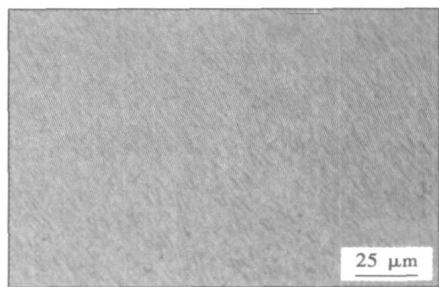


图5 焊缝区 β 晶粒内部显微组织

Fig. 5 Microstructure in β -grain of weld zone

2.2.3 热影响区

热影响区整体形貌如图6所示. 从图6中可以看出, 随着与焊缝中心距离的不同, 组织形态有一定的区别. 在距离焊缝区较近的I区, 焊接过程中温度较高, 温度达到了 β 相变温度以上, 冷却过程中发生了再结晶过程, 生成了晶粒细小的等轴 β 相. 而在靠近焊缝较远的II区, 则为长条状的 β 晶粒.

离焊缝区最远的 III 区, β 晶界不明显.

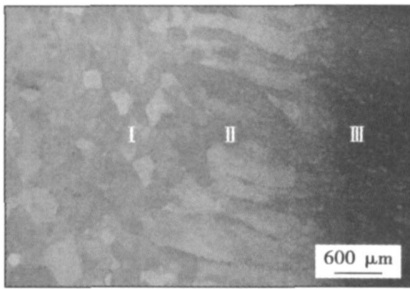
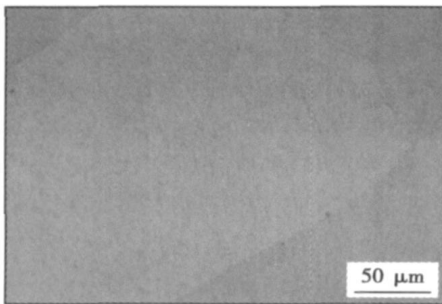


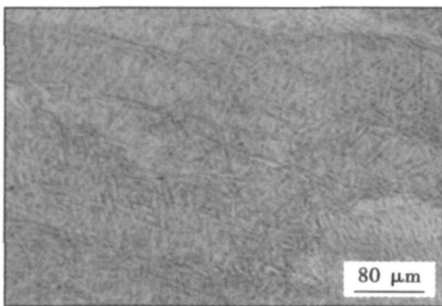
图 6 热影响区整体形貌

Fig. 6 Whole configuration of HAZ

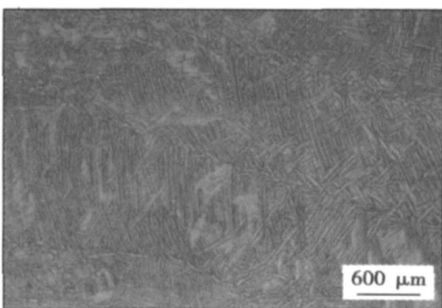
图 7 为热影响区各区域的显微组织形貌. 图 7a 显示等轴晶内部为针状的马氏体 α' 相, 弥散分布在



(a) I 区



(b) II 区



(c) III 区

图 7 热影响区不同区域显微组织形貌

Fig. 7 Microstructure in various regions of HAZ

亚稳的 β 相基体内. 图 7b 显示 II 区内为针状和片状 α 相束分布于 β 基体形成的魏氏组织. 图 7c 显示 III 区晶粒形态与母材类似, 但晶内和晶界 α 相发生了一定程度的聚集长大.

2.2.4 熔合区

熔合区位于热影响区与焊缝区之间, 是接头在焊接过程中固相与液相的分界区, 因此该区域最容易出现气孔、未熔合的焊接缺陷. 图 8 为试验接头熔合区的显微组织形貌, 从图中可以看出该区域结合良好, 热影响区的等轴 β 晶粒与焊缝区的柱状 β 晶粒联生, 从而保证了接头的可靠连接.

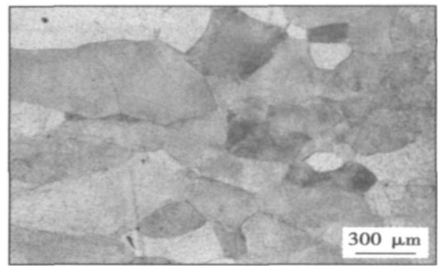


图 8 熔合区显微组织形貌

Fig. 8 Microstructure of fusion zone

2.3 接头力学性能

2.3.1 抗拉强度及断后伸长率

图 9 为焊缝不同厚度部位抗拉强度与断后伸长率的比较. 从图 9 中可以看出不同部位的接头抗拉强度与断后伸长率基本相同, 在厚度方向上几乎没有差异. 断裂都发生于距离焊缝较远的母材处, 说明接头的强度达到或者超过了母材的强度. 但接头断后伸长率与母材相比严重下降, 只达到母材的 50% 左右. 接头拉伸时颈缩主要发生在母材上, 而焊缝处基本没有发生变形, 说明焊缝的塑性较差.

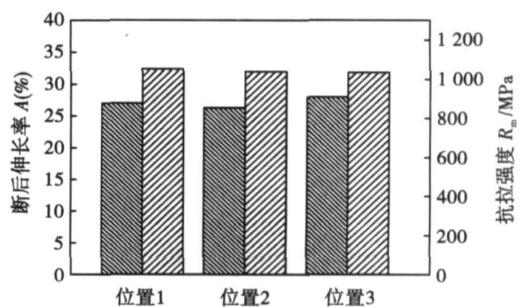


图 9 接头不同部位抗拉强度和断后伸长率对比

Fig. 9 Comparison of tensile strength and elongation between various loactions of joint

2.3.2 显微硬度

对接头横截面垂直方向和中部水平方向的显微硬度分布进行了测量,如图10所示.从图10a可见在垂直方向,硬度基本无差异,这与拉伸试验结果一致.从图10b可以看出,由于焊缝区相组成为 α' 针状马氏体,硬度最高;而热影响区, I 区为再结晶的 β 相内分布有少量的针状马氏体,硬度略微下降, II 区内的魏氏组织也属于脆性组织,故硬度也高于母材.而在 III 区,则由于片状 α 相的长大,从而使该区域发生软化,硬度明显降低.

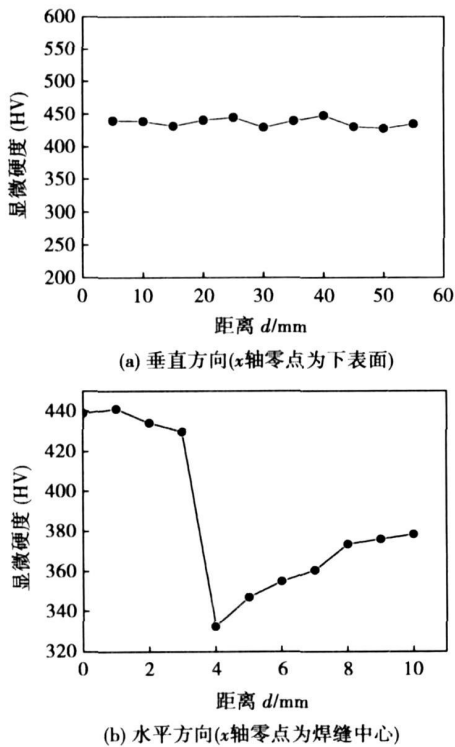


图10 焊缝横截面显微硬度分布

Fig. 10 Microhardness distribution in cross-section of joint

3 结 论

(1) 采用电子束成功焊接了56 mm厚TC21钛合金,接头强度达到母材水平,厚度方向性能一致.但接头塑性损失较大,断后伸长率只达到母材的50%左右.

(2) 接头焊缝区组织形态为以柱状 β 晶粒为基

体,针状的马氏体 α' 相弥散在其中;热影响区从焊缝到母材分为三个区域,依次为等轴再结晶 β 晶粒区、片状和针状 α 相形成的魏氏组织区、片状 α 相聚集长大的区域.熔合区内柱状晶与热影响区的等轴晶共生.

(3) 接头焊缝区硬度最高,其次是热影响区的等轴晶区和魏氏组织区,而热影响区内片状 α 相聚集长大的区域硬度值最低.

参考文献:

- [1] Boyer R R. An overview on the use of titanium in the aerospace industry [J]. *Materials Science and Engineering A*, 1996, 213(1-2): 103-114.
- [2] Caiazzo F, Curcio F, Daurelio G, *et al.* Ti6Al4V sheets lap and butt joints carried out by CO₂ laser: mechanical and morphological characterization [J]. *Journal of Materials Processing Technology*, 2004, 149(1-3): 546-552.
- [3] 许鸿吉, 尹丽香, 李晋炜, 等. TC4钛合金电子束焊接接头组织和性能[J]. *焊接学报*, 2005, 26(11): 43-46.
Xu Hongji, Yin Lixiang, Li Jinwei, *et al.* Microstructures and properties of TC4 alloy joints welded by the electron beam welding [J]. *Transactions of the China Welding Institution*, 2005, 26(11): 43-46.
- [4] 付鹏飞, 黄锐, 刘方军, 等. TA12钛合金电子束焊接组织性能及残余应力分析[J]. *焊接学报*, 2007, 28(2): 82-84.
Fu Pengfei, Huang Rui, Liu Fangjun, *et al.* Microstructure and residual stress of TA12 titanium alloy with electron beam welding [J]. *Transactions of the China welding institution*, 2007, 28(2): 82-84.
- [5] 王利发, 刘建中, 胡本润. TA15钛合金电子束焊接接头力学性能[J]. *焊接学报*, 2007, 27(1): 97-100.
Wang Lifa, Liu Jianzhong, Hu Benrun. Mechanical properties of TA15 titanium alloy electron beam welded joint [J]. *Transactions of the China Welding Institution*, 2007, 27(1): 97-100.
- [6] 陈志勇, 王清江, 刘建荣, 等. Ti-60钛合金电子束焊接接头高温下的失效与变形行为[J]. *金属学报*, 2008, 44(3): 263-271.
Chen Zhiyong, Wang Qingjiang, Liu Jianrong, *et al.* Failure and deformation behaviors of electron beam weldment of titanium alloy Ti-60 at elevated temperature [J]. *Acta Metallurgica Sinica*, 2008, 44(3): 263-271.

作者简介: 张秉刚, 男, 1971年出生, 博士, 副教授. 研究方向为新材料及异种材料的电子束焊接. 发表论文20余篇.

Email: zhangbg@hit.edu.cn

MAIN TOPICS, ABSTRACTS & KEY WORDS

Tele-operated TIG welding robot for hyperbaric underwater pipeline repair welding

JIAO Xiangdong¹, ZHOU Canfeng¹, XUE Long¹, GAO Hui¹, FANG Xiaoming² (1. Research Center of Joining Technology in Ocean Engineering, Beijing Institute of Petrochemical Technology, Beijing 102617, China; 2. China Offshore Oil Engineering Co. LTD., Tianjin 300452, China). p 1—4

Abstract: Among the available underwater pipeline repair methods hyperbaric TIG welding technology may be the easier one to obtain better joint quality. Due to the low automation level and the bevel preparation difficulty, the repair welding should be conducted based on both the welding knowledge of the welder on deck and the operation skill of the diver. A tele-operated robot for all position hyperbaric pipe welding was developed. In the specified case of underwater welding, the process was controlled by a surface based operator, a clear and real time image of the arc as well as the image of groove location were required. An observation system of three cameras for chamber, groove and weld was also developed respectively. All the necessary message of vision, welding current and arc voltage were collected and transferred to the surface by the developed computerized information system. The underwater pipeline maintenance system consists of the welding robot, observation system, the information system, together with the habitation. The chamber gas type, the welding power source and arc striking were also studied. With the welding procedure developed in the hyperbaric welding laboratory, a good weld was obtained in a underwater pipe repair welding test at Bohai sea.

Key words: tele-operated robot; underwater welding; underwater pipeline repairing; welding robot

Electron beam welding of TC21 titanium alloy with large thickness

ZHANG Binggang¹, WANG Ting¹, CHEN Guoqing¹, LIU Chenglai², LIU Yulong¹ (1. State Key Laboratory of Advanced Welding Production Technology, Harbin Institute of Technology, Harbin 150001, China; 2. Shenyang Liming Aero-Engine (Group) Co. LTD., Shenyang 110000, China). p 5—8

Abstract: Electron beam welding of TC21 56 mm titanium alloy was carried out. The microstructure and the mechanical properties of welded joints were analyzed and tested. The results showed that the weld zone consisted of the columnar β grains, and in which the transgranular acicular α' martensite were dispersedly distributed. HAZ can be divided into three parts from base metal to weld zone, which are the equiaxed recrystallized β grain zone, Widmanstatten structure zone formed by lamellar and acicular α phases and lamellar α phase coarsening zone. Fusion zone consists of the adnate columnar and equiaxed grains. Tensile strength of joints reaches to that of base metal and the failure appears in the base metal. The mechanical properties are uniform along the vertical direction. Plasticity in the welded joint is greatly decreased and only up to 50% of that of the base metal. The microhardness in weld zone is the highest, and that of the equiaxed grain zone and Widmanstatten structure zone in HAZ is higher, and the microhardness in columnar α phase coarsen-

ing zone is the lowest.

Key words: TC21 titanium alloy; electron beam welding; microstructure; mechanical properties

Hardness and microstructure of China low activation martensitic steel fusion welded joint

LEI Yucheng¹, GU Kangjia¹, ZHU Qiang¹, CHEN Xizhang¹, JU Xin², CHANG Fenghua³ (1. School of Materials Science and Engineering, Jiangsu University, Zhenjiang 212013, Jiangsu, China; 2. Physics Department, University of Science and Technology of Beijing, Beijing 100083, China; 3. Harbin Welding Training Institute, Harbin 150046, China). p 9—12

Abstract: The preheated and non-preheated 4 mm China low activation martensitic steel (CLAM) plate were welded by TIG welding and post-weld heat treating, and the hardness and microstructure in welded joint were tested and observed. The results show that the hardness in the weld metal is higher and the softening band appears in the heat-affected zone (HAZ) closing to the base metal. The tempered lath martensite is observed in welded joints. There is no significant difference in martensite content between the preheated and non preheated weldments. A large amount of carbide particles are observed in the grains and at the grain boundary. The carbides are small rods in weld metal and large granular in the HAZ and base metal respectively. The microstructure and carbides in welded joints have great effect on the hardness.

Key words: China low activation martensitic steel; hardness; martensite; carbide

Numerical analysis on stress distribution in adhesive-welded double lap joint of aluminum

YOU Min¹, LI Zhi^{1,2}, ZHAO Meirong¹, GUO Bin², YAN Jialing¹ (1. Hubei Key Laboratory of Hydroelectric Machinery Design & Maintenance, China Three Gorges University, Yichang 443002, Hubei, China; 2. Mechanical and Electric Engineering Department, China Three Gorges Project Corporation, Yichang 443002, Hubei, China). p 13—16

Abstract: The influence of the elastic modulus of adhesives and nuggets position on the stress distribution in adhesive-welded double lap joints of aluminum was investigated by elastic-plastic finite element method (FEM). The results obtained show that the influence of the elastic modulus of adhesive on the stress distribution in adhesive-welded double lap joints of aluminum is significant. The load subjected by the nuggets is greater when the elastic modulus of adhesive is lower and the load subjected by the adhesive layer increases when the elastic modulus of adhesive is higher. The effect of nuggets location is also significant when the center of the nugget is moved to the left end of the overlap zone. The peak stress along the mid-bonding line of the aluminum double lap joint increases when the center of the nuggets are moved to near the left end of the overlap zone. The peak value of the von mises equivalent stress increases from 55.2 MPa to 77.4 MPa when the nugget center is shifted from the point at 12.5 mm to 5.5 mm. Therefore, the load bearing ability of the adhesive-welded double lap joints of aluminum can be im-